MNRAS **000**, 1–9 (2011) Preprint 26 September 2021 Compiled using MNRAS LATEX style file v3.0

The mode selection problem in δ Scuti stars

L. A. Balona
South African Astronomical Observatory, P.O. Box 9, Observatory, Cape Town, South Africa

Accepted .... Received ...

ABSTRACT
Inspection of the periodograms of 9597 *TESS* δ Scuti stars indicates that there is little, if any, correlation between the frequencies and location of the stars in the H–R diagram. A quantitative measure of similarity is described which can be used to compare two frequency spectra. When applied to non-adiabatic pulsation models, the expected strong correlation is found between the predicted pulsation frequencies for models with similar temperatures and luminosities. The correlation is maintained when rotational splitting is included. However, no correlation is found between the frequencies of *TESS* δ Scuti stars with similar effective temperatures and luminosities. As suspected, the observed frequencies do not depend on the stellar parameters, contradicting the models. This result suggests that an unknown mode selection process is active, presenting a fundamental problem in our current understanding of pulsational driving or the structure of the outer layers of stars with radiative atmospheres.

Key words: stars:oscillations; stars:variables:δ Scuti.

1 INTRODUCTION

The δ Scuti stars are main sequence A or F stars which vary in light with multiple coherent frequencies. They are the most common type of pulsating variable. δ Sct stars in which all significant frequency peaks in the periodogram are below $5\,\mathrm{d}^{-1}$ are called γ Doradus variables. It is, however, likely that the driving mechanism in the γ Dor stars is the same as in the δ Sct stars (Balona 2018).

Guzik (2021) has presented an excellent review of the δ Sct stars, but fails to mention what is perhaps the most perplexing problem. This is the fact that δ Sct stars with very similar global parameters appear to have very different pulsation frequencies and amplitudes. This perception soon arises after visual inspection of a few hundred periodograms, but is difficult to quantify. For instance, the effect of rotation cannot easily be evaluated.

It is taken for granted that unstable pulsation frequencies must change smoothly with small changes in the global parameters. Yet, there are many δ Sct stars where just one frequency peak dominates the spectrum. In the same region of the H–R diagram, there are also many δ Sct stars with very rich frequency spectra. One has to ask the question of how such a dramatic difference in frequency distribution can occur when the stars have very similar effective temperatures and luminosities. It is also difficult to understand why some stars with similar global parameters pulsate as δ Sct variables, while others appear to be non-pulsating. The impression is that an unknown mechanism is at play in which some modes are damped while others are enhanced. This is the "mode selection problem" (Balona 2018).

In this paper, a quantitative definition of similarity between two frequency distributions is presented. The method is applied to unstable modes in non-adiabatic pulsation models. As expected, models with similar parameters lead to quantitatively similar frequency distributions of the unstable modes. It is shown that the method is insensitive to rotation rate.

The same method is applied to *TESS* observations of δ Sct stars. It is shown that there is no correlation at all between periodograms of stars with similar parameters, nor can the difference be attributed to differences in rotation rate. In fact, the results seem to imply that the observed modes in δ Sct stars are selected by an entirely random process. This result points to a fundamental problem in stellar pulsation theory or modeling of the outer layers of these stars.

2 DATA AND METHODOLOGY

The data used here are from sectors 1–41 of the *TESS* mission. Each sector consists of about 27 d of continuous photometry with 2-min cadence. While stars near the ecliptic equator are only observed for one sector, stars near the ecliptic poles are observed in every sector. The light curves are corrected for instrumental signatures and long-term drift. These are called pre-search data conditioning (PDC) light curves.

As each sector becomes available, the light curve and periodogram of each star with $T_{\rm eff} > 6000\,\mathrm{K}$ is visually examined and classified according to variability type. As can be

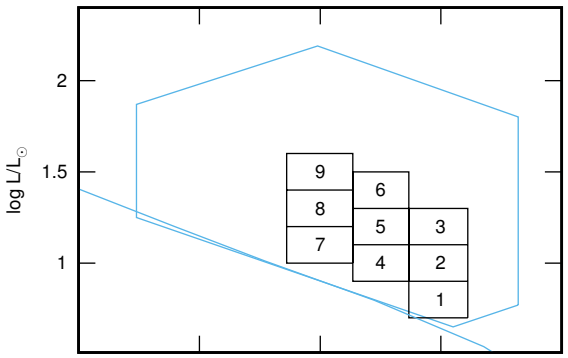

Figure 1. The theoretical H–R diagram showing the approximate location of the δ Scuti instability region (polygon) and the zero-age main sequence. The numbered boxes are the regions discussed in the text.

expected, most of the variables are of the δ Sct type. Among the 82000 stars already classified, there are 9597 δ Sct stars.

Effective temperatures, $T_{\rm eff}$, of these stars were obtained from the literature. Where possible, estimates from spectroscopic modelling are used. The stellar luminosity, $\log L/L_\odot$, was estimated from *Gaia* ERD3 parallaxes (Gaia Collaboration et al. 2016, 2018) in conjunction with reddening obtained from a three-dimensional map by Gontcharov (2017) using the bolometric correction calibration by Pecaut & Mamajek (2013). Periodograms of each star were calculated and frequencies extracted.

The correlation between two periodograms can then be taken as a measure of similarity. We denote the amplitude of periodogram, i, sampled with equal frequency spacing $\delta\nu$ by $y_i(\nu)$ and the amplitude of a template periodogram, j, by $y_j(\nu)$. The correlation coefficient, r, between frequencies ν_1 and ν_2 is

$$r = \frac{1}{A_i A_j} \sum_{\nu=\nu_1}^{\nu_2} y_i(\nu) y_j(\nu) \delta\nu,$$

where A_i, A_j are constants. The values of these constants are chosen so that correlating a periodogram with itself gives unity:

$$A_i^2 = \sum_{\nu=\nu_1}^{\nu_2} y_i^2(\nu) \delta\nu.$$

The value of r then lies between $r = 0$ (no similarity) and $r = 1$ (periodograms are identical).

Given any two stars, neither the pulsation frequencies nor the amplitudes will be exactly the same. When the periodogram peaks are very narrow, the correlation between the two periodograms is likely to be close to zero, even if the two periodograms are nearly identical. To avoid this problem, it is necessary to broaden the frequency peaks. This will allow some overlap of the periodogram peaks, leading to a non-zero correlation. The broader the peaks, the greater the correlation, but the lower the power of discrimination. It is thus necessary to establish a compromise in the broadening parameter.

In practice, the extracted frequencies and amplitudes are used, rather than the periodogram itself. Each frequency is broadened by a Gaussian with the same broadening parameter, σ, for all stars. The appropriate value for σ depends on the range of frequency variation that is expected within the small region of the H–R diagram where stars may be considered to have similar physical parameters. This can be estimated from pulsation models as discussed below. The broadened frequency spectrum is sampled at 1000 equally spaced frequency points between $\nu_1 = 5\,{\rm d}^{-1}$ and $\nu_2 = 100\,{\rm d}^{-1}$. The lower limit was chosen to avoid variability due to rotation or eclipses.

Table 1. Location of the regions discussed in the text. The number of *TESS* δ Sct stars, $N_{\rm strs}$, and the number of models, $N_{\rm mod}$, in each region is given. The last two columns give the fraction of stars where only one dominant frequency peak is visible and the fraction of stars with rich frequency spectra.

Region	$T_{\rm eff}$	$\log L/L_\odot$	$N_{\rm strs}$	$N_{\rm mod}$	$f_{\rm DOM}$
1	6900 - 7300	0.70 - 0.90	159	15	0.19
2	6900 - 7300	0.90 - 1.10	622	3	0.13
3	6900 - 7300	1.10 - 1.30	491	12	0.11
4	7300 - 7700	0.90 - 1.10	1060	3	0.06
5	7300 - 7700	1.10 - 1.30	611	9	0.07
6	7300 - 7700	1.30 - 1.50	308	9	0.06
7	7700 - 8200	1.00 - 1.20	957	5	0.06
8	7700 - 8200	1.20 - 1.40	463	8	0.07
9	7700 - 8200	1.40 - 1.60	260	16	0.09

In order to compare stars with similar global parameters, the instability strip needs to be divided into suitably small regions. The size of these regions can be estimated from the approximate uncertainties in $T_{\rm eff}$ and $\log L/L_\odot$. The typical uncertainty in the effective temperature is about 100–200 K. The typical error in $\log L/L_\odot$ is about 0.05–0.10 dex, allowing for errors of 0.02 mag in the apparent magnitude, 0.10 mag in visual extinction and 0.02 mag in the bolometric correction in addition to the parallax error. With these considerations in mind, the δ Sct instability strip was divided into nine regions as shown in Fig. 1 and Table 1. The placement of these regions is motivated by the distribution of δ Sct stars observed by *TESS* (Fig. 2).

3 PULSATION MODELS

Evolutionary stellar models were computed using the Warsaw - New Jersey evolution code (Paczyński 1970), assuming an initial hydrogen fraction, $X_0 = 0.70$ and metal abundance, $Z = 0.020$ and using the chemical element mixture of Asplund et al. (2009) and OPAL opacities (Rogers & Iglesias 1992) Overshooting from the convective core was not included. A mixing length parameter $\alpha_{\rm MLT} = 1.0$ was adopted for the convective scale height. All models are non-rotating. The non-adiabatic code developed by Dziembowski (1977b) was used to obtain the pulsation frequencies and growth rates.

Pulsations in these models are purely driven by the opacity κ mechanism operating in the He II partial ionisation region. More advanced models, such as those by Xiong et al. (2016) include driving due to convective effects and predict rather different frequency distributions. The purpose of these models is to demonstrate the fundamental assumption that underlies all such models: that the frequencies which are

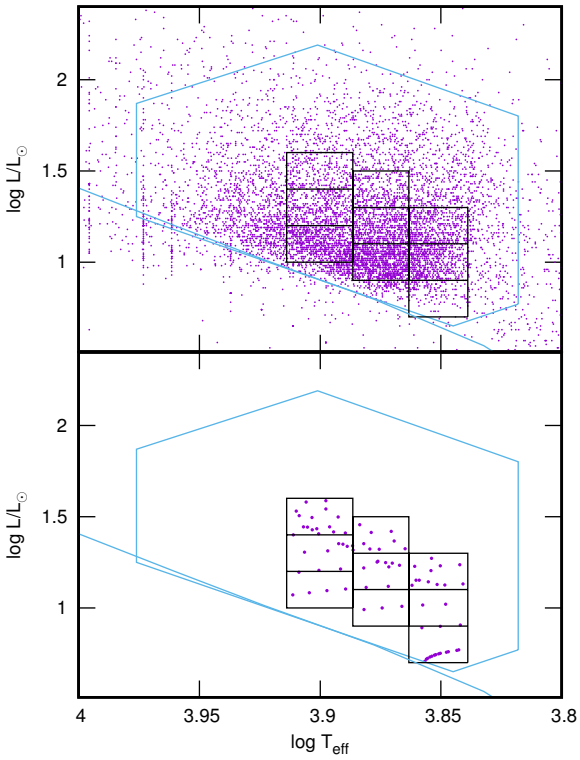

Figure 2. The top panel is theoretical H–R diagram showing individual δ Sct stars (points), the approximate location of the instability region (polygon), and the zero-age main sequence. The numbered boxes are the regions discussed in the text. The bottom panel is the same except that the points show the location of individual stellar models discussed in the text.

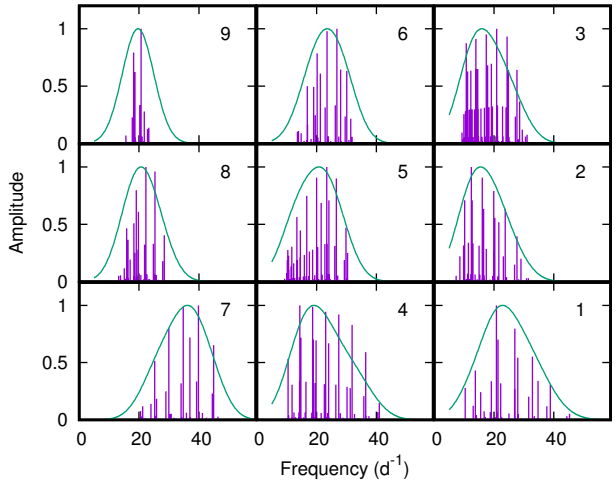

Figure 3. Frequencies from models in nine regions (labeled) and the corresponding distribution obtained by convolving the frequencies by a Gaussian with $\sigma = 5\,\mathrm{d}^{-1}$ (curve).

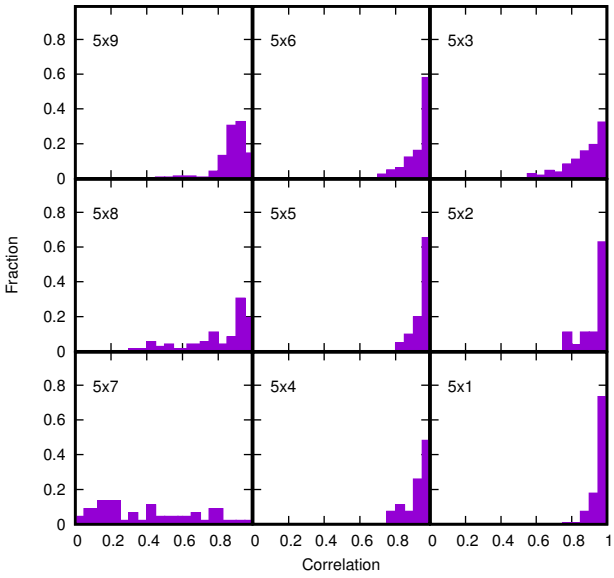

Figure 4. Distribution of correlation between region 5 and surrounding regions (labeled) for no rotation.

driven depend only on the effective temperature, luminosity and chemical composition. Since these vary smoothly from model to model, one expects similar frequencies to be driven in models within the same region in the H–R diagram.

Amplitudes play a fundamental role in defining the frequency distribution. Currently, there are no models which are able to predict the equilibrium amplitudes of non-radial modes. One option is to set the amplitude to the growth rate if it is positive, or to zero if negative. However, there is no guarantee that the growth rate can be used as a measure of the final amplitude. This is determined by unknown nonlinear interactions. Another option is to set all modes with positive growth rates to some constant value. Both choices lead to the same result.

The mode visibility, and hence the observed amplitude, also depends on the spherical harmonic degree, l, and the angle of inclination. This factor is roughly approximated by the value of b_l as tabulated in Dziembowski (1977a). As will be shown below, it is not important how the amplitude is chosen as any choice will show that the models predict similar frequencies for stars with similar stellar parameters.

The distribution of the models in the instability region is shown in the bottom panel of Fig. 2. The frequencies of a given mode can be obtained as a function of $T_{\rm eff}$ and $\log L/L_\odot$. For fixed spherical harmonic degree and radial order, the rms scatter in the frequencies within each region is typically in the range 2–6 d^{-1}. This can be higher for g modes or mixed modes. A Gaussian broadening of $\sigma = 5\,\mathrm{d}^{-1}$ was selected, but the results are not sensitive to the value of σ.

Amplitudes proportional to the growth rate, η, were used. These amplitudes were corrected for the visibility factor, b_l, but no attempt was made to model the angle of inclination. Examples of frequency spectra for modes with $l \leq 4$ and $\eta > 0$ are shown in Fig. 3 for models in nine different regions. Each frequency peak is convolved by a Gaussian with $\sigma = 5.0\,\mathrm{d}^{-1}$, giving the envelope shown in the same figure.

The convolved frequencies for a given model were cross-correlated with every model in the same region, as well as with models in all the other regions. For example, if region 5 (9 models) is cross-correlated with region 9 (16 models), the result will be 144 correlation coefficients. The distribution of

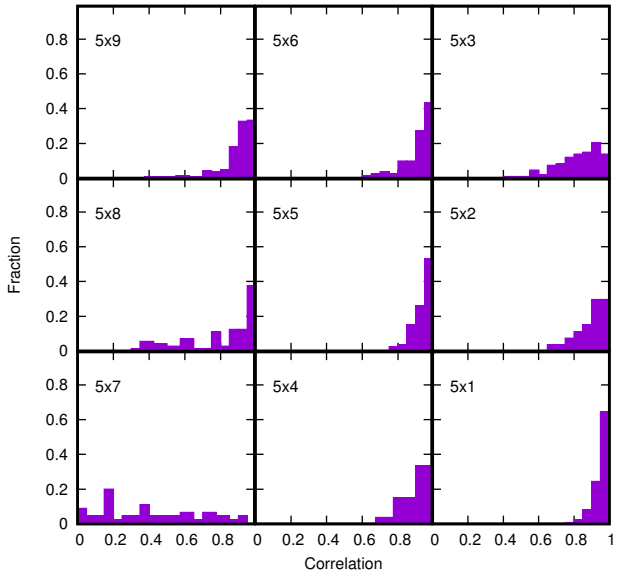

Figure 5. Distribution of correlation between region 5 and surrounding regions (labeled) for simulated rotational splitting.

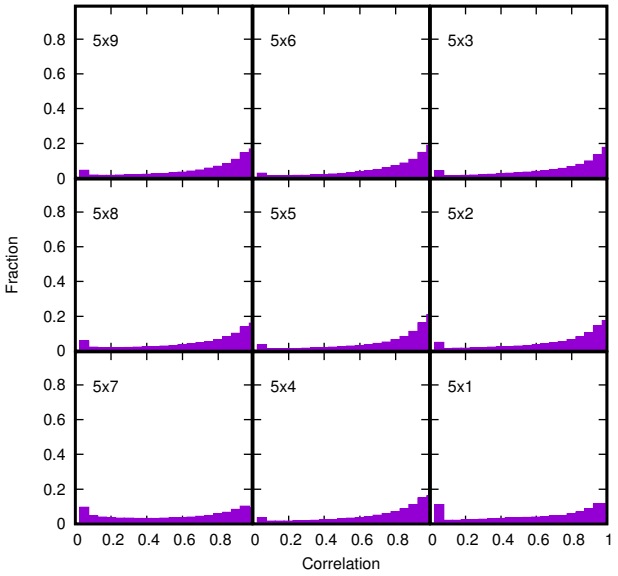

Figure 6. Distribution of correlation between region 5 and surrounding regions (labeled) for *TESS* δ Sct stars.

these correlation coefficients is shown in the panel marked 5×9 in Fig 4.

Fig 4 shows, for example, that models in regions 1, 2 and 6 have unstable modes with frequency spectra closely resembling those of models in region 5, while models in region 7 appears to have significantly different frequency distributions from models in region 5. There is nothing surprising in this: it is what one would expect if models with similar parameters give rise to similar frequency distributions.

It may come a surprise, however, that there is more similarity in the frequency spectra between models in regions 5 and 1 than models within region 5 itself. This has to do with two models in region 5 near the boundary with model 4. These have rather different frequency distributions from the remaining models in region 5 because their luminosities are quite significantly lower than the other models in the same region.

Rotation has the effect of introducing additional frequency peaks. These fill in the gaps in pulsation frequency in non-rotating stars. The overall effect is to broaden the frequency distribution by an amount roughly proportional to the rotational frequency. This follows from the fact that a mode of degree l is split into $2l+1$ multiplets. For low rotation rates, the frequency splitting is given by $C\Omega$, where C is Ledoux's constant and Ω the rotation frequency. Equal frequency splitting breaks down for moderate to rapid rotation, but the overall effect is still a broadening of the envelope of the frequency peaks in the non-rotating case. Since a broadening of the frequency distribution increases the chance of overlap with the frequency distribution of another star, the effect of rotation is to increase the correlation between frequency distributions.

To test the effect of rotation, frequency splitting was applied to each unstable mode in the models, so that the central non-rotating frequency, ν, was replaced by $2l+1$ frequencies of equal amplitude and equal spacing centered on ν. The frequency spacing was determined in accordance with the known distribution of rotational velocities in A stars (Balona 2019). This spacing is typically in the range $\delta\nu$ =0–3 d^{-1} with an average of about 0.5 d^{-1}. As in the non-rotating case, the frequency distribution was convolved using a Gaussian with $\sigma = 5\,\mathrm{d}^{-1}$.

The resulting distribution of correlation coefficients is shown in Fig. 5. There is hardly any difference between these distributions and those of the non-rotating models in Fig. 4. Further tests with increased frequency splitting lead the same result. It is concluded that rotation has no significant effect on the distribution of correlation coefficients, making the test of similarity insensitive to rotation.

4 OBSERVATIONS

From 9597 δ Sct observed by *TESS*, 4931 stars were used to determine the similarity of frequency distributions in stars with approximately the same stellar parameters. Table 1 lists the numbers of δ Sct stars in each region.

According to our expectations, most of the stars in region 5 should have similar frequency distributions. The distribution of correlation coefficients should therefore have a strong peak near $r = 1$. One expects weaker correlations for more distant regions. This, any rate, is the expectation and would be no surprise. Instead, Fig 6 shows almost no correlation at all, neither within region 5 itself nor with any of the neighbouring regions.

In fact, the resulting distributions compare very well with what one might expect for a random distribution. A random distribution of frequency spectra can be obtained by using the same stars, but placing them at random within any of the nine regions. Fig. 7 shows that the resulting distributions of correlation coefficients are very similar to those in Fig. 6. It can be concluded that there is no link at all between the observed frequencies in a δ Sct star and its location in the H–R diagram. While this result might appear

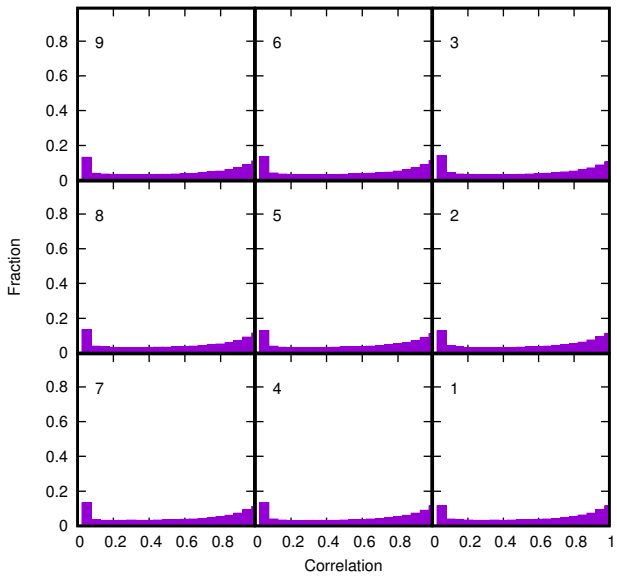

Figure 7. Distribution of correlations between frequency spectra of stars in the labeled region with frequency spectra of stars in randomly chosen regions.

surprising, and is at odds with pulsation models, it accords with the impression that is obtained by visual inspection of the periodograms. The periodogram of each star appears to be unique.

5 PERIODOGRAMS OF INDIVIDUAL STARS

A selection of periodograms of *TESS* δ Sct stars is shown in Figs. 8, 9 and 10 to illustrate some important points. For this purpose, 8 stars with just a single dominant peak and 8 stars with fairly rich frequency spectra (or other interesting features) were selected in each region.

The single-mode stars are those which do not have peaks higher than one-fifth of the amplitude of the main peak. For most regions, about 7% of the stars are single-mode, but the fraction approaches 20% among the coolest stars (Table 1). For these stars, the mean $\langle v \sin i \rangle = 76 \pm 7\,\mathrm{km\,s^{-1}}$, while for all δ Sct stars $\langle v \sin i \rangle = 108 \pm 3\,\mathrm{km\,s^{-1}}$. It seems that single-mode stars rotate more slowly than the δ Sct stars in general. This may be a factor in the selection of a single mode but, if so, the selection mechanism is not known.

A rich frequency spectrum cannot be obtained from rotational splitting of a star with just a single mode. The fact that stars with single modes and with multiple modes can exist within the same region of the H–R diagram cannot be explained by current models. Clearly there is an unknown mode selection process at play.

Note also that the frequencies of the single-mode stars within a given region are very different. This means that the single frequency peaks must belong to different modes in each star, even though the stars have much the same $T_{\rm eff}$ and $\log L/L_\odot$. This, again, cannot be understood with current models.

Pulsation models always predict driving in a rather wide range of frequencies (e.g. Xiong et al. 2016). No pulsation model can account for just a single pulsation mode. Of course, there could be very many modes which are below the detection level, but the problem then shifts to explaining why one mode has a much higher amplitude than the others.

The single-mode stars in the figures are not high-amplitude δ Sct stars (HADS). The HADS are essentially single- or double-mode stars with harmonics and combination frequencies. HADS were thought to be high-luminosity giant stars intermediate between δ Sct and Cepheid variables. In the interior of such stars, high-frequency p modes behave like high-order g modes. The large number of spatial oscillations of these modes in the deep interior leads to severe radiative damping. As a result, nonradial modes are damped. However, Balona (2018) showed that the HADS observed by *Kepler* are not intermediate between δ Sct and Cepheid variables. The single-mode stars presented here are of low amplitude and do not have detectable harmonics or combination frequencies.

6 CONCLUSIONS

The huge variety of frequency distributions in δ Sct stars in the same region of the H–R diagram has been a puzzle for many years (Balona 2018). Inspection of many hundreds of periodograms gives the strong impression that each δ Sct star has a unique set of frequencies, unrelated to its location in the H–R diagram and probably unrelated to rotation rate. On the other hand, non-adiabatic pulsation models predict that stars with the same global parameters and rotation rates should pulsate with the same set of frequencies. This apparent mismatch between theory and observation may point to a fundamental problem in our understanding of stellar pulsation and the outer layers of stars.

In this paper, the degree of similarity between two sets of frequencies is measured by a correlation coefficient. Frequencies predicted from non-adiabatic pulsation models are found to be strongly correlated when the models have similar effective temperatures and luminosities. The correlation drops as the difference in temperature and luminosity increases. In other words, the unstable frequencies predicted by the models are strongly linked to the location of the model in the H–R diagram. The correlation coefficients are insensitive to rotational splitting.

When applied to a sample of 4931 *TESS* δ Sct stars with known effective temperatures and luminosities, no correlation at all is found between the frequencies of stars with similar effective temperatures and luminosities. In other words, the observed frequencies are not related in any way to the location of the star in the H–R diagram. In fact, they seem to obey a random distribution. This is contrary to model predictions, but verifies the impression obtained by visual inspection of the periodograms.

A mosaic of 144 periodograms consisting of 8 periodograms with only a single dominant frequency peak and 8 periodograms showing multiple frequency peaks are presented for each region. While this cannot do justice to the full data set, it serves to illustrate the above conclusion. Within the same region of the H–R diagram, stars with just one dominant mode co-exist with stars with very rich frequency spectra. Stars with single frequency peaks are to be found at all locations in the instability strip. Current models

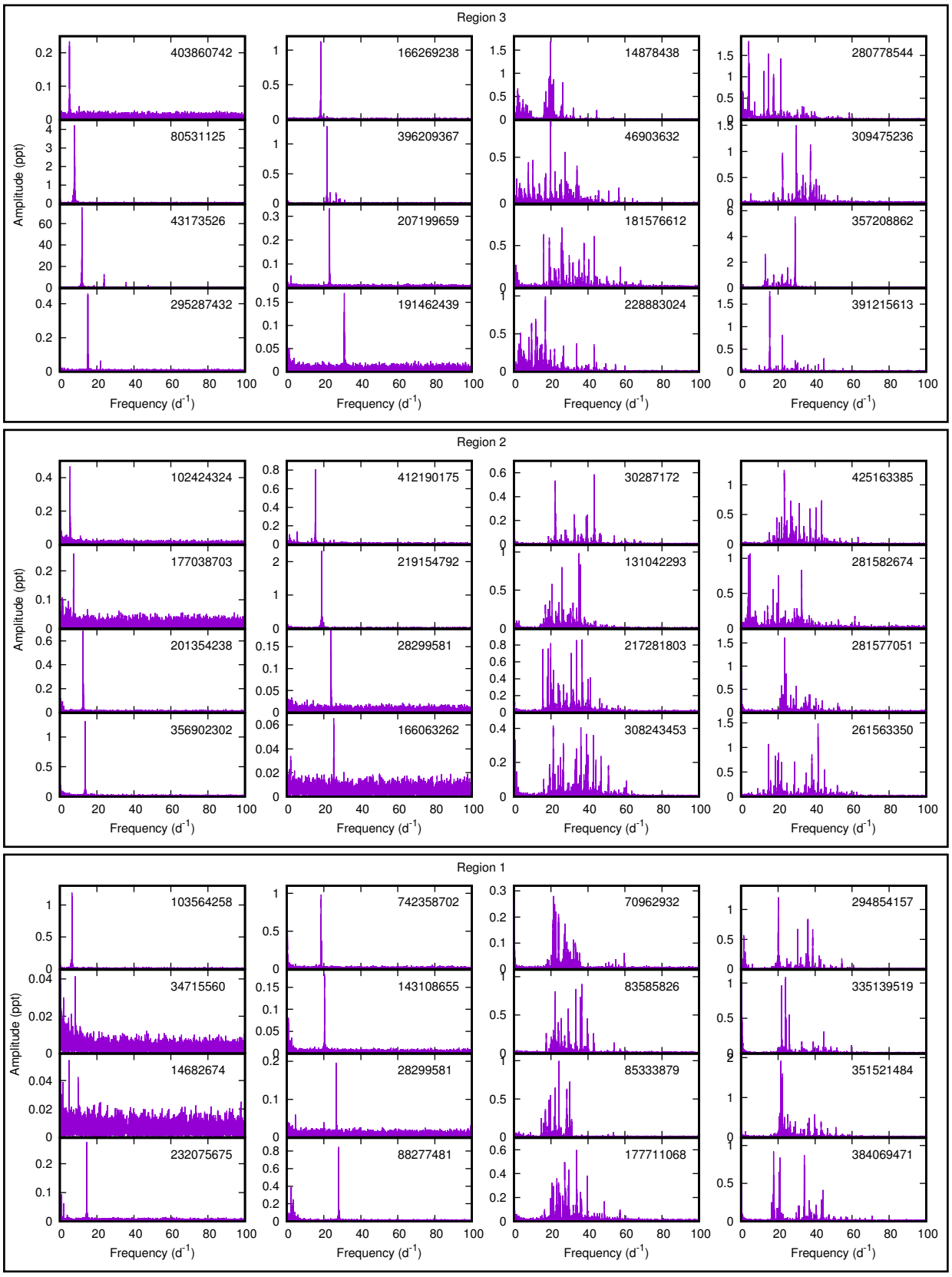

Figure 8. Periodograms of some stars. Top: region 3, middle: region 2, bottom: region 1.

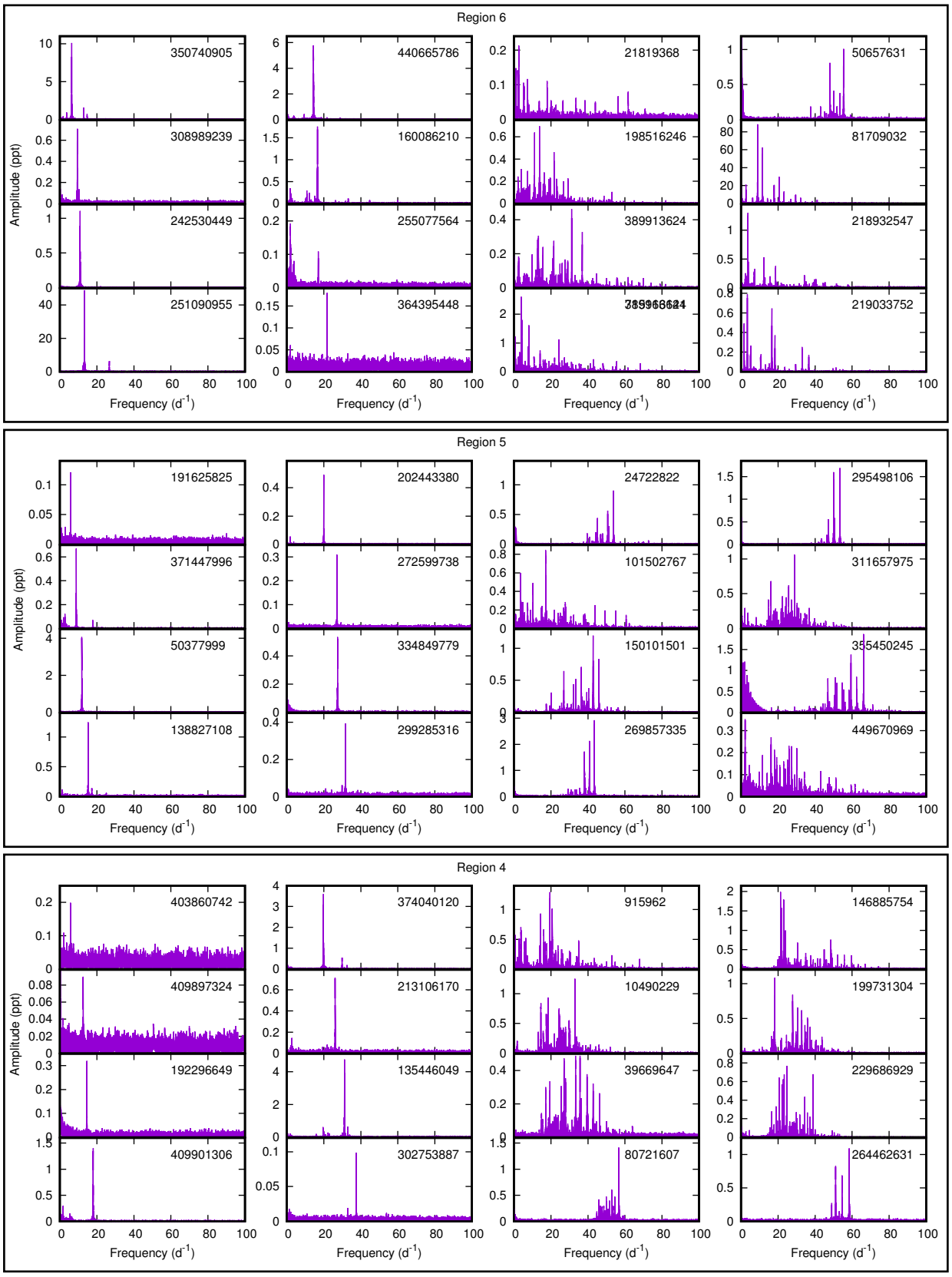

Figure 9. Region 4,5,6: periodograms of some stars.

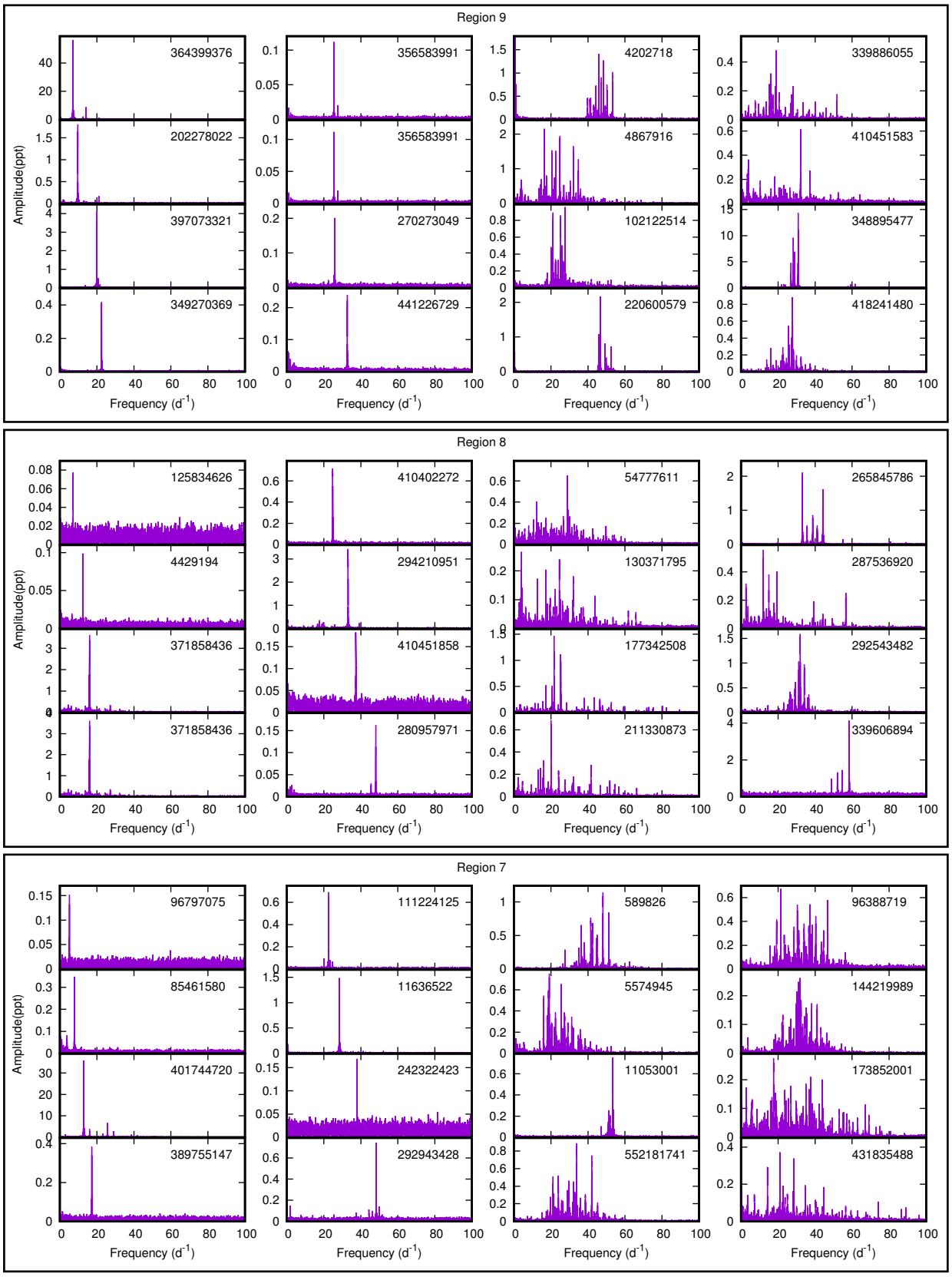

Figure 10. Region 7,8,9: periodograms of some stars.

predict a range of unstable frequencies and cannot account for single frequencies. This suggests that an unknown mode selection process is active.

While non-adiabatic models fail to predict the observed frequencies, the adiabatic eigenfrequencies themselves are not affected. In other words, asteroseismology based on model calculations will still be valid. It is perhaps the driving mechanism itself or the non-linear growth to full amplitude that require further study. Unfortunately, nonlinear, nonradial pulsation calculations are beyond present capabilities.

The effect described here may also apply to other self-driven nonradial pulsating stars such as the β Cep variables. The likely presence of starspots and even flares on early-type stars (Balona 2021) suggests that our current understanding of the outer stellar layers and the atmospheres of A and B stars is incomplete. Further investigations along these lines will probably be required to shed light on the mode selection processes that seem to be present in δ Sct stars.

DATA AVAILABILITY

The data underlying this article are available in the article.

ACKNOWLEDGMENTS

I thank the National Research Foundation of South Africa for financial support and Dr. W. Dziembowski for permission to use his code.

This paper includes data collected by the *TESS* mission. Funding for the *TESS* mission is provided by the NASA Explorer Program. Funding for the *TESS* Asteroseismic Science Operations Centre is provided by the Danish National Research Foundation (Grant agreement no.: DNRF106), ESA PRODEX (PEA 4000119301) and Stellar Astrophysics Centre (SAC) at Aarhus University. We thank the *TESS* and TASC/TASOC teams for their support of the present work.

This work has made use of data from the European Space Agency (ESA) mission Gaia (https://www.cosmos.esa.int/gaia), processed by the Gaia Data Processing and Analysis Consortium (DPAC, https://www.cosmos.esa.int/web/gaia/dpac/consortium). Funding for the DPAC has been provided by national institutions, in particular the institutions participating in the Gaia Multilateral Agreement.

This research has made use of the SIMBAD database, operated at CDS, Strasbourg, France. This research has made use of the VizieR catalogue access tool, CDS, Strasbourg, France (DOI: 10.26093/cds/vizier). The original description of the VizieR service was published in A&AS 143, 23.

The data presented in this paper were obtained from the Mikulski Archive for Space Telescopes (MAST). STScI is operated by the Association of Universities for Research in Astronomy, Inc., under NASA contract NAS5-2655.

REFERENCES

Asplund M., Grevesse N., Sauval A. J., Scott P., 2009, ARA&A, 47, 481
Balona L. A., 2018, MNRAS, 479, 183
—, 2019, MNRAS, 490, 2112
—, 2021, Frontiers in Astronomy and Space Sciences, 8, 32
Dziembowski W., 1977a, Acta Astronomica, 27, 203
—, 1977b, Acta Astron., 27, 95
Gaia Collaboration, Brown A. G. A., Vallenari A., Prusti T., de Bruijne J. H. J., Babusiaux C., Bailer-Jones C. A. L., 2018, ArXiv e-prints
Gaia Collaboration, Prusti T., de Bruijne J. H. J., et al., 2016, A&A, 595, A1
Gontcharov G. A., 2017, Astronomy Letters, 43, 472
Guzik J. A., 2021, Frontiers in Astronomy and Space Sciences, 8, 55
Paczyński B., 1970, Acta Astron., 20, 47
Pecaut M. J., Mamajek E. E., 2013, ApJS, 208, 9
Rogers F. J., Iglesias C. A., 1992, ApJS, 79, 507
Xiong D. R., Deng L., Zhang C., Wang K., 2016, MNRAS, 457, 3163